Petroleum Science 22 (2025) 1125–1139

Contents lists available at ScienceDirect

Petroleum Science

journal homepage: www.keaipublishing.com/en/journals/petroleum-science

Original Paper

Adaptive subtraction with 3D U-net and 3D data windows to suppress seismic multiples

Jin-Qiang Huang [a], Li-Yun Fu [b], Jia-Hui Ma [c], Xing-Zhong Du [d], Zhong-Xiao Li [c,*], Ke-Yi Sun [c]

[a] College of Resources and Environmental Engineering, Key Laboratory of Karst Georesources and Environment (Guizhou University), Ministry of Education, Guiyang, 550025, Guizhou, China
[b] School of Geosciences, China University of Petroleum (East China), Qingdao, 266580, Shandong, China
[c] Department of Electronic Engineering, School of Electronic Information, Qingdao University, Qingdao, 266071, Shandong, China
[d] Power China Guiyang Engineering Corporation Limited, Guiyang, 550081, Guizhou, China

ARTICLE INFO

Article history:
Received 13 June 2024
Received in revised form
21 September 2024
Accepted 24 January 2025
Available online 28 January 2025

Edited by Meng-Jiao Zhou

Keywords:
Adaptive subtraction
3D U-net
3D data windows
Transfer learning
Multiple suppression

ABSTRACT

The deep convolutional neural network U-net has been introduced into adaptive subtraction, which is a critical step in effectively suppressing seismic multiples. The U-net approach has higher precision than the traditional linear regression approach. However, the existing 2D U-net approach with 2D data windows can not deal with elaborate discrepancies between the actual and simulated multiples along the gather direction. It may lead to erroneous preservation of primaries or generate obvious vestigial multiples, especially in complex media. To further enhance the multiple suppression accuracy, we present an adaptive subtraction approach utilizing 3D U-net architecture, which can adaptively separate primaries and multiples utilizing 3D windows. The utilization of 3D windows allows for enhanced depiction of spatial continuity and anisotropy of seismic events along the gather direction in comparison to 2D windows. The 3D U-net approach with 3D windows can more effectively preserve the continuity of primaries and manage the complex disparities between the actual and simulated multiples. The proposed 3D U-net approach exhibits 1 dB improvement in the signal-to-noise ratio compared to the 2D U-net approach, as observed in the synthesis data section, and exhibits more outstanding performance in the preservation of primaries and removal of residual multiples in both synthesis and reality data sections. Moreover, to expedite network training in our proposed 3D U-net approach we employ the transfer learning (TL) strategy by utilizing the network parameters of 3D U-net estimated in the preceding data segment as the initial network parameters of 3D U-net for the subsequent data segment. In the reality data section, the 3D U-net approach incorporating TL reduces the computational expense by 70% compared to the one without TL.
© 2025 The Authors. Publishing services by Elsevier B.V. on behalf of KeAi Communications Co. Ltd. This is an open access article under the CC BY-NC-ND license (http://creativecommons.org/licenses/by-nc-nd/4.0/).

1. Introduction

The effective suppression of seismic multiples is crucial in seismic exploration of oil and gas prior to the seismic imaging with primaries (Verschuur, 2013; Ma et al., 2024a; Ma et al., 2024b; Wang et al., 2021). Seismic primaries manifest as singular reflections at the subsurface layers, while multiples encompass a multitude of reflections (Verschuur and Berkhout, 1997; Ma et al., 2009; Liu et al., 2018). The commonly employed approach for suppressing multiples begins with the simulation of multiples (Li et al., 2021; Wang et al., 2023a,b). Effective suppression of multiples necessitates adaptive subtraction of simulated multiples from the initial recorded data, considering the intricate disparities in amplitude, time and space between the actual and simulated multiples (Guitton and Verschuur, 2004; Li et al., 2023a). This process of adaptive subtraction plays a pivotal role in achieving effective multiple suppression.

At present, deep neural networks have been widely used in seismic data processing, such as denoising (Wang et al., 2019), seismic waveform classification (Zhao et al., 2019), arrival picking of microseismic signals (Zhang and Sheng, 2020; Sheng et al., 2022),

* Corresponding author.
E-mail address: thulzx@163.com (Z.-X. Li).

https://doi.org/10.1016/j.petsci.2025.01.010
1995-8226/© 2025 The Authors. Publishing services by Elsevier B.V. on behalf of KeAi Communications Co. Ltd. This is an open access article under the CC BY-NC-ND license (http://creativecommons.org/licenses/by-nc-nd/4.0/).

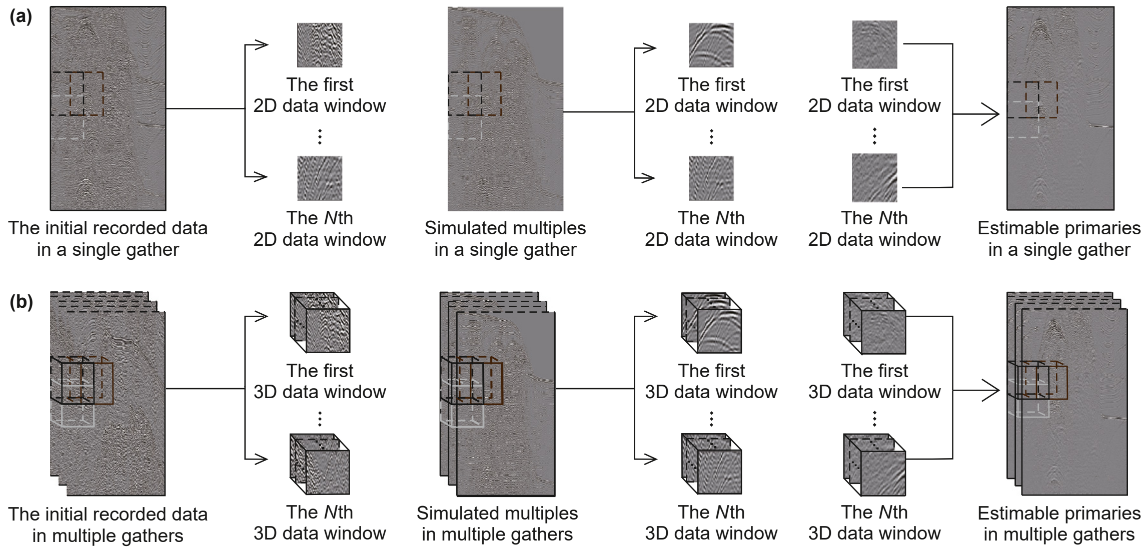

Fig. 1. Illustration of splitting the seismic gathers into data windows and merging data windows into seismic gathers. **(a)** 2D data windows. **(b)** 3D data windows.

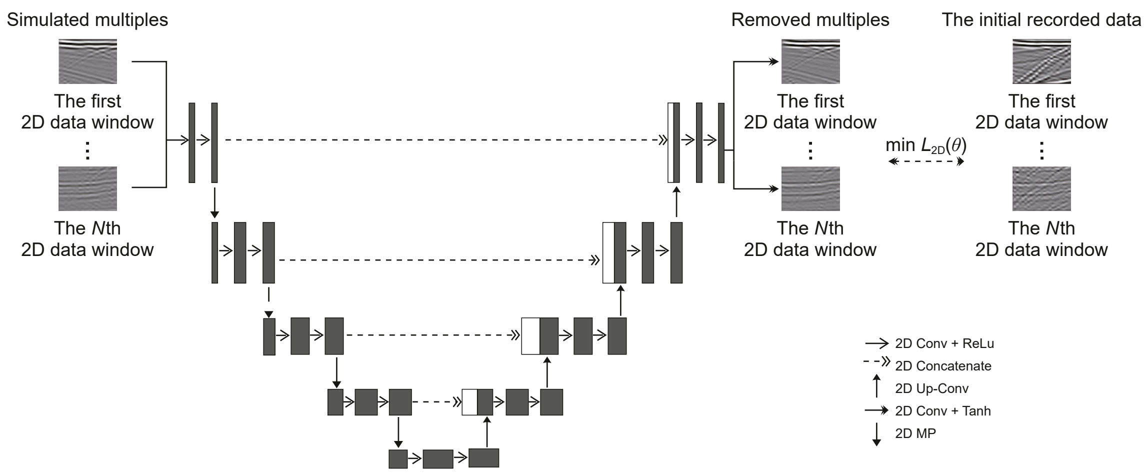

Fig. 2. Illustration of 2D U-net. L_{2D} indicates loss functions of the 2D U-net approach.

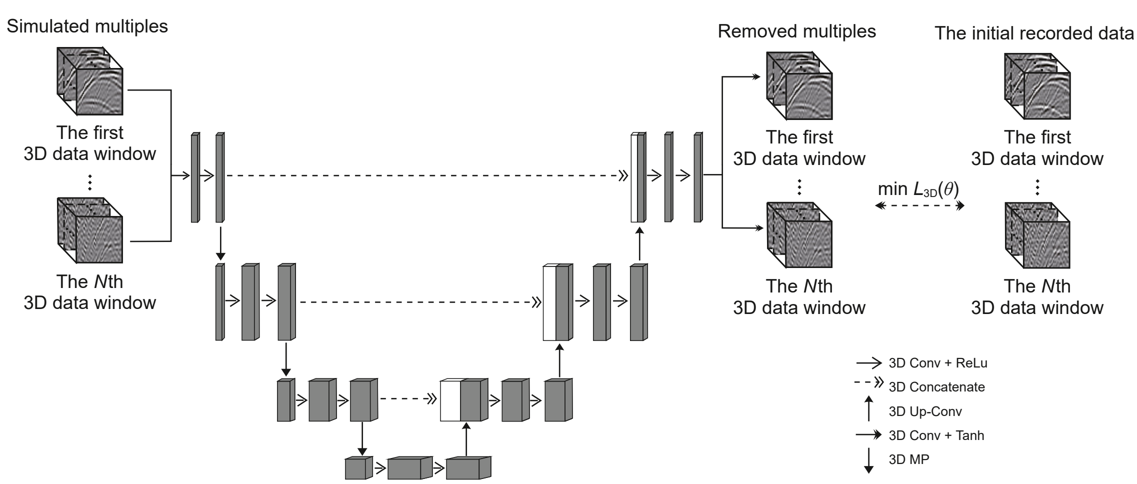

Fig. 3. Illustration of 3D U-net. L_{3D} indicates loss functions of the 3D U-net approach.

seismic facies interpretation (Yang et al., 2023), sensitivity analysis of shale gas production (Xue et al., 2024). The application of deep learning in seismic multiple suppression has become prevalent (Mousavi and Beroza, 2022; Song et al., 2021). To achieve adaptive subtraction within the non-linear regression (non-LR) framework, the 2D U-net approach has been introduced as an effective approach (Li et al., 2021; Wang et al., 2023a,b). The input data in this approach consists of 2D windows of simulated multiples, while the reference data comprises 2D windows of initial recorded data. This implies that the simulated multiples are matched with the initial recorded data (Li et al., 2021; Ma et al., 2024b). The 2D U-net approach lacks the capability to precisely express the elaborate discrepancies between the actual and simulated multiples along the gather direction. The aforementioned limitation may consequently result in incorrect preservation of primaries or cause residual multiples. To address this deficiency, we propose the 3D U-net approach.

Instead of using 2D windows for the 2D U-net, the proposed 3D U-net approach utilizes 3D windows which are formed by multiple 2D windows in adjacent gathers. The 3D windows can effectively represent the spatial continuity and anisotropy of seismic events along the gather direction (Wu et al., 2019; Li and Li, 2018). The utilization of 3D network modules (Mehta and Arbel, 2018) and 3D windows in the 3D U-net approach enhances the preservation of primary continuity and enables accurate characterization of discrepancies between the actual and simulated multiples along the gather direction. Therefore, the proposed 3D U-net approach provides growing protection for primaries and exhibits superior performance in eliminating residual multiples compared to the 2D U-net approach.

Adjacent seismic data segments exhibit comparable disparities between simulated and true multiples. Transfer learning (TL) theory has been used to expedite the 2D U-net approach (Siahkoohi et al., 2019; Li et al., 2023c). In this paper we employ the TL to use the network parameters of 3D U-net in preceding data segment as the initial network parameters for training 3D U-net of the subsequent data segment. The 3D U-net does not require being retrained with random initial network parameters for each data segment except for the first data segment. In this way the proposed 3D U-net approach can be expedited with reduced epoch number of network training.

The subsequent sections of this paper are organized as follows. Firstly, we will proffer the theoretical framework about the 3D U-net approach. Subsequently, we will assess the efficacy of the 3D U-net approach through its application to both synthesis and reality datasets. Lastly, we will provide a concluding summary for this paper.

2. Theory

2.1. The 2D U-net approach

The initial recorded data and simulated multiples are partitioned to create multiple 2D data windows of size $n \times n$ prior to conducting adaptive subtraction (Li et al., 2021). Fig. 1(a) gives the illustration of splitting the seismic gathers into 2D windows, which are used to train the 2D U-net. The mathematical model of the 2D U-net approach is described as follows (Li et al., 2021):

$$\mathbf{P}_{2D} = \mathbf{S}_{2D} - U_{2D}(\overline{\mathbf{M}}_{2D}; \mathbf{\Theta}_{2D}) \tag{1}$$

where the matrixes $\mathbf{P}_{2D}$, $\mathbf{S}_{2D}$ and $\overline{\mathbf{M}}_{2D}$ represent the estimable primaries, initial recorded data and simulated multiples in a 2D window respectively. $U_{2D}(\cdot)$ indicates 2D U-net and its network parameters are represented by $\mathbf{\Theta}_{2D}$. Fig. 2 depicts the architecture of 2D U-net, using the simulated multiples as input data and initial recorded data as reference data. The 2D U-net comprises numerous down-sampling and up-sampling stages (Ronneberger et al., 2015; Senapati et al., 2023). The fundamental 2D network modules of each down-sampling stage comprise 2D convolution (Conv), Rectified Linear Unit (ReLu), and 2D Max Pooling (MP). The fundamental 2D network modules of each up-sampling stage comprise 2D transposed convolution (Up-Conv), 2D Conv, and ReLu. In each down-sampling stage the number of 2D convolutional kernels is doubled and in each up-sampling stage the number of 2D Up-Conv kernels is halved. The final convolutional layer has the activation function of Tanh to make the amplitude of the output lie between −1 and 1. Moreover, the symmetric down-sampling and up-sampling feature windows are concatenated in Fig. 2.

The loss function utilized for training 2D U-net is outlined as follows (Li et al., 2021):

$$L_{2D}(\Theta) = \sum_{i=1}^{P}\left[||\mathbf{S}_{2D,i} - U_{2D}(\overline{\mathbf{M}}_{2D,i}; \mathbf{\Theta}_{2D})||_1 + \mu||\mathbf{\Theta}_{2D}||_2^2 \right] \tag{2}$$

where $\boldsymbol{\mu}$ is the regularization factor and $\boldsymbol{P}$ is denoted as the batch size. The Adam algorithm (Kingma and Ba, 2015) is implemented to iteratively compute the network parameters $\mathbf{\Theta}_{2D}$ by minimizing Eq. (2). After the training of 2D U-net the estimable primaries in 2D data windows are merged as seismic gathers in Fig. 1(a).

2.2. The proposed 3D U-net approach

The 3D windows are formed by arranging multiple 2D windows in adjacent gathers along the gather direction (Wu et al., 2019; Li and Li, 2018). Fig. 1(b) illustrates the splitting of the seismic gathers of the initial recorded data and simulated multiples into 3D data windows for training 3D U-net. The 3D U-net approach's

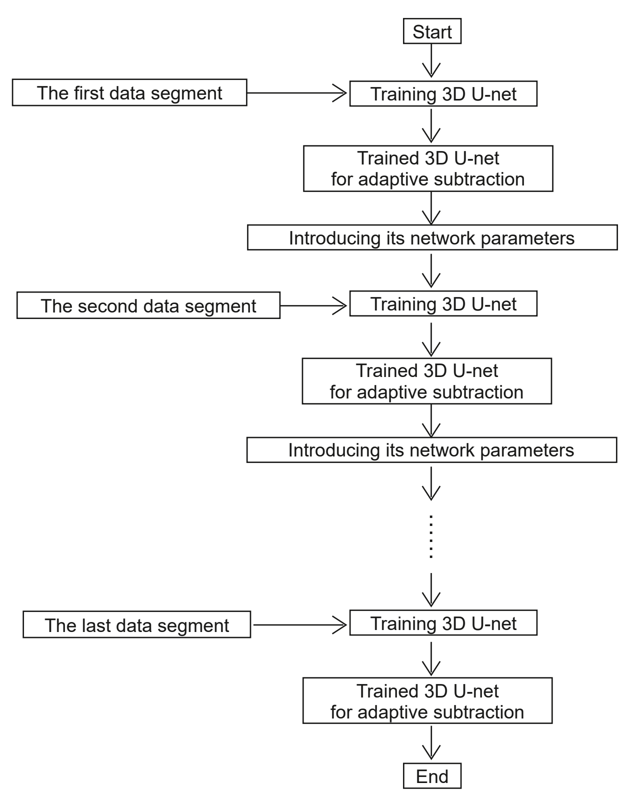

Fig. 4. Flowchart of the 3D U-net method with TL.

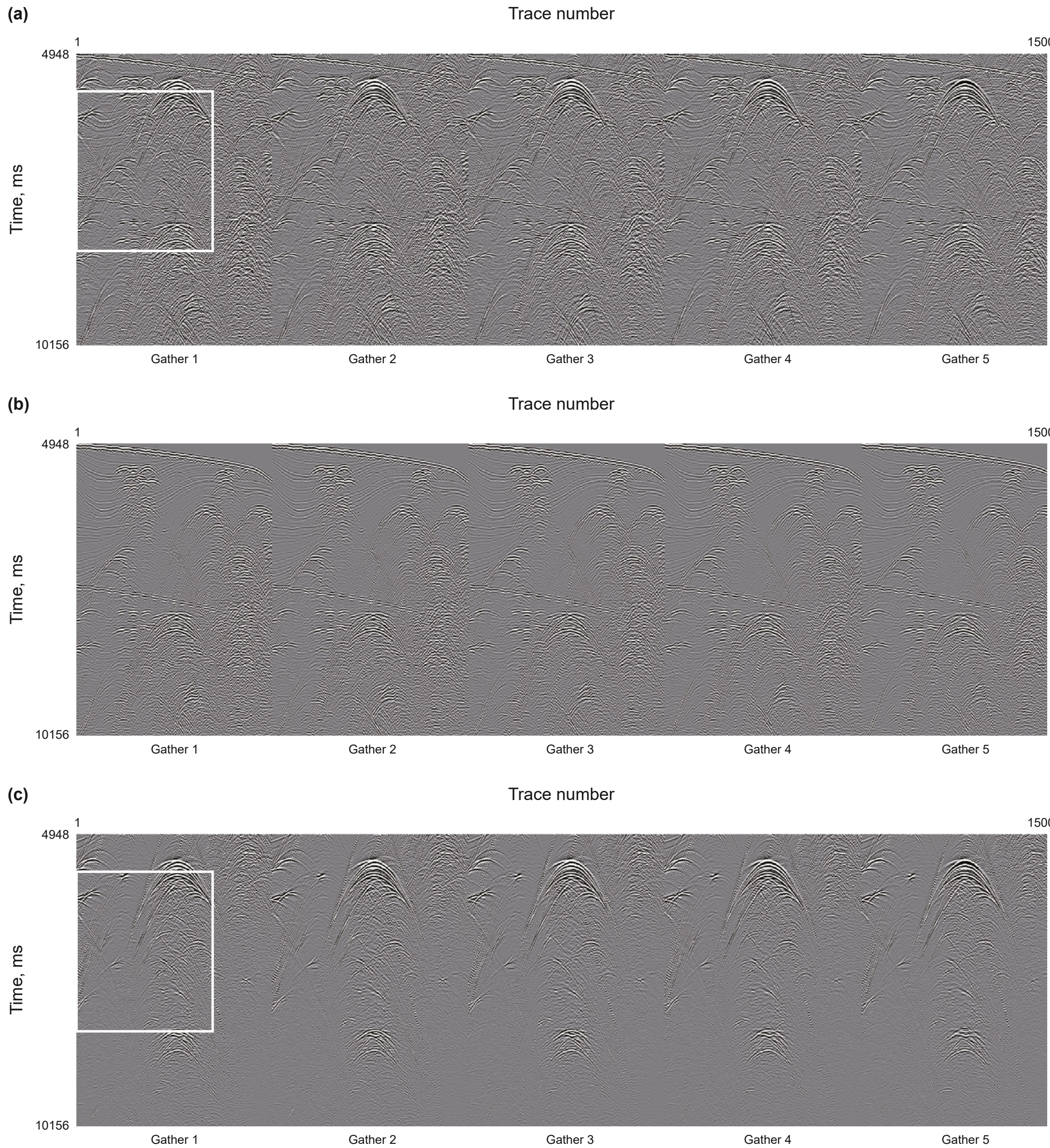

Fig. 5. Synthesis data example in five gathers. **(a)** The initial recorded data. **(b)** Simulated multiples by 2D SRME. (c) Actual primaries.

mathematical model is presented as follows:

$$\mathbf{P}_{3\mathrm{D}} = \mathbf{S}_{3\mathrm{D}} - U_{3\mathrm{D}}(\overline{\mathbf{M}}_{3\mathrm{D}}; \mathbf{\Theta}_{3\mathrm{D}}) \tag{3}$$

where the matrixes $\mathbf{P}_{3\mathrm{D}}$, $\mathbf{S}_{3\mathrm{D}}$ and $\overline{\mathbf{M}}_{3\mathrm{D}}$ represent the estimable primaries, initial recorded data and simulated multiples in a 3D window respectively. $U_{3\mathrm{D}}(\cdot)$ indicates 3D U-net (Mehta and Arbel, 2018) and its network parameters are represented by $\mathbf{\Theta}_{3\mathrm{D}}$.

The architecture of the 3D U-net utilized in this paper is depicted in Fig. 3, wherein the input data comprises 3D windows of simulated multiples and the reference data consists of 3D windows of the initial recorded data. Both the 2D U-net and 3D U-net have the same network architecture of down-sampling and up-sampling steps. However, compared with 2D U-net, 3D U-net has 3D network modules, such as 3D Conv, ReLu, 3D MP and 3D Up-Conv in Fig. 3.

The following loss function is defined for training 3D U-net:

$$L_{3\mathrm{D}}(\mathbf{\Theta}_{3\mathrm{D}}) = \sum_{i=1}^{B} \left[\left\| \mathbf{S}_{3\mathrm{D},i} - U_{3\mathrm{D}}(\overline{\mathbf{M}}_{3\mathrm{D},i}; \mathbf{\Theta}_{3\mathrm{D}}) \right\|_1 + \lambda \left\| \mathbf{\Theta}_{3\mathrm{D}} \right\|_2^2 \right] \tag{4}$$

where the regularization factor is denoted as λ and the batch size is denoted as B. During the network training the Adam algorithm is applied for estimating the network parameters $\mathbf{\Theta}_{3\mathrm{D}}$ through the minimization of the loss function $L_{3\mathrm{D}}(\mathbf{\Theta}_{3\mathrm{D}})$. The L1 norm minimization constraint is applied to preserve primaries effectively (Guitton and Verschuur, 2004; Li et al., 2021). Numerous 3D windows generated by multiple gathers are utilized for conducting self-supervised training without actual primaries as labels. After the training of 3D U-net the 3D data windows of estimable primaries are merged into seismic gathers as illustrated in Fig. 1(b).

The 2D U-net approach employs 2D network modules and conducts adaptive multiple subtraction in 2D data windows (Li

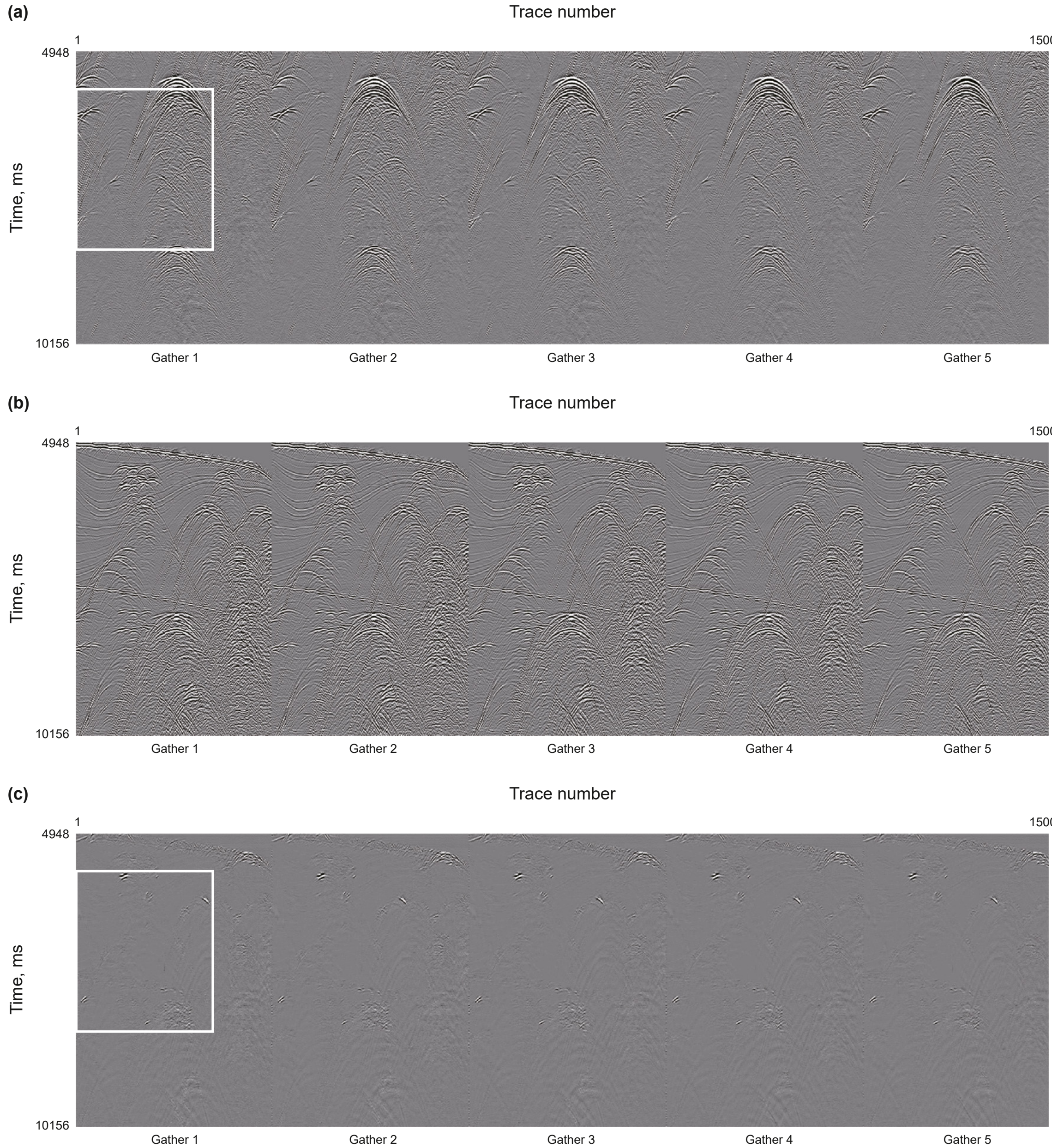

Fig. 6. Synthesis data example in five gathers. **(a)** Estimable primaries of the 2D U-net approach. **(b)** Removed multiples of the 2D U-net approach. **(c)** Difference gathers gotten by subtracting Fig. 6(a) from Fig. 5(c).

et al., 2021). The 3D windows can better represent the spatial continuity and anisotropy of seismic events along the gather direction than the 2D windows. The 3D U-net approach utilizing 3D network modules can effectively protect primaries and eliminate residual multiples by simultaneously employing multiple 3D windows for adaptive subtraction, surpassing the capabilities of the 2D U-net approach.

2.3. Flowchart of proposed 3D U-net approach

The 3D U-net approach consists of two stages: training and prediction, which are similar with those of the 2D U-net approach. In the training stage the 3D U-net is trained using 3D windows comprising both the initial recorded data and simulated multiples. In the subsequent prediction stage the trained 3D U-net is employed to generate estimated multiple by inputting 3D windows containing simulated multiples. The identical 3D data windows of the simulated multiples are utilized for both the training and prediction procedures. Estimated primaries are achieved by directly subtracting the estimated multiples from the initial recorded data.

In this paper seismic gathers are sequentially partitioned into many data segments. Within each segment the seismic gathers are further divided into 3D data windows. Similar discrepancies between the simulated and true multiples are observed across adjacent data segments. The introduction of TL involves utilizing the previously estimated network parameters of the 3D U-net in previous data segment as the initial parameters for training 3D U-net in the subsequent data segment. This process is illustrated in Fig. 4. To ensure the convergence of the training loss curve, the proposed 3D U-net approach sets the epoch number to R in the first data segment and K in subsequent data segment. We have $K \ll R$ by introducing the TL theory. The proposed 3D U-net approach with TL

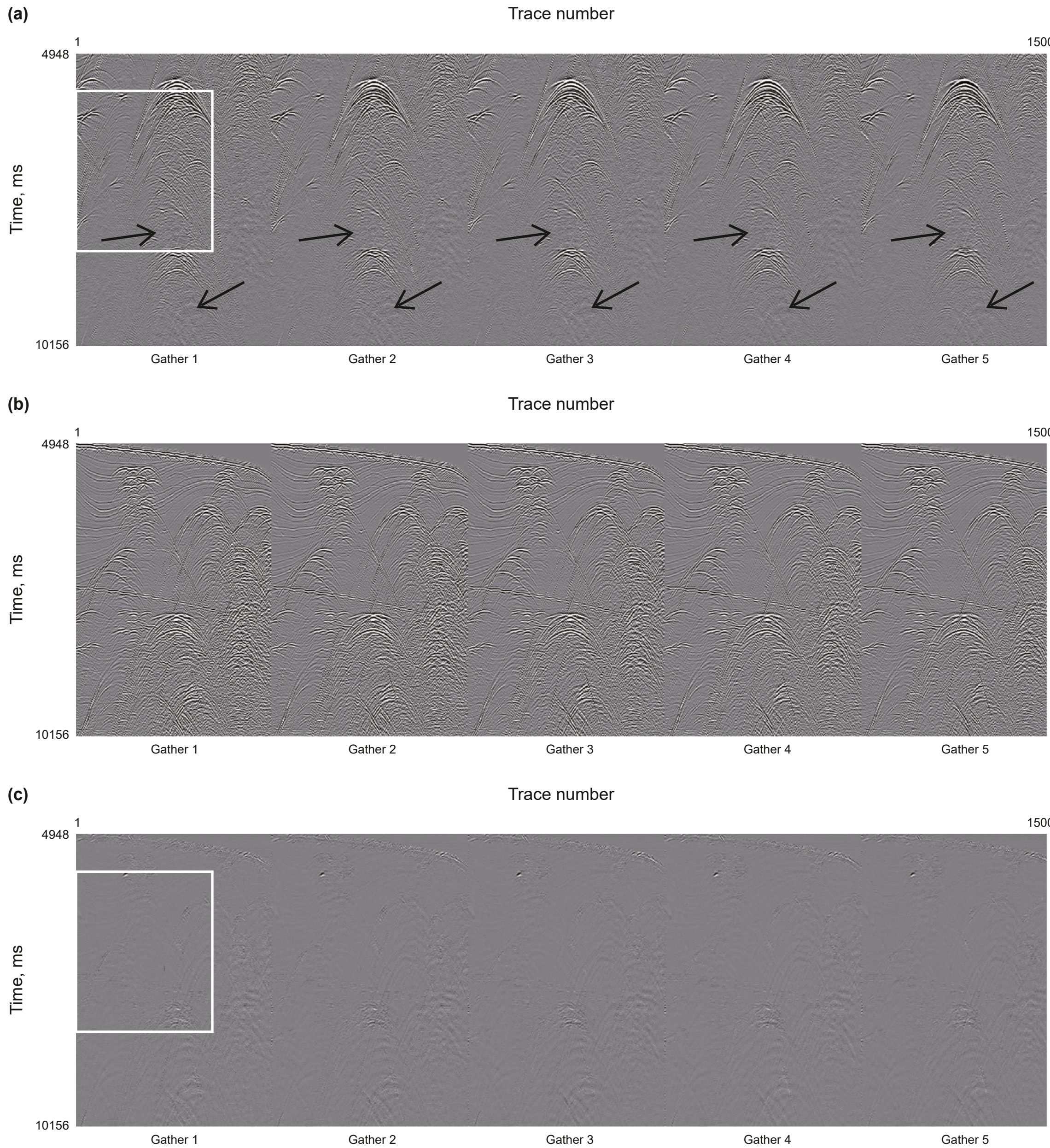

Fig. 7. Synthesis data example in five gathers. **(a)** Estimable primaries of the 3D U-net approach. **(b)** Removed multiples of the 3D U-net approach. **(c)** Difference gathers gotten by subtracting Fig. 7(a) from Fig. 5(c).

can enhance computational efficiency effectively by reducing the epoch number compared with the one without TL.

Furthermore, over-matching exists in all adaptive subtraction approaches. By minimizing the loss function in Eq. (4) there is potential risk of over-matching to primaries for the 3D U-net approach. The effectiveness of adaptive subtraction for each data segment is contingent upon when the training process is terminated and how the hyper-parameters are selected for network training. The appropriate number of epochs is carefully selected to ensure complete convergence of the training loss curve. Ample data windows are utilized for 3D U-net training, network parameters are regularized, and L_1 norm minimization constraint is applied to primaries. Additionally, the number of 3D convolution kernels is set appropriately in the first down-sampling step to avoid the risk of over-matching to primaries (Li et al., 2021). Therefore, we choose the network hyper-parameters by trial and error. Improper selection of these hyper-parameters may harm primaries or result in residual multiples. We employ initial settings for each hyper-parameter and gradually adjust its value to compare the effectiveness of multiple suppression results. The optimal values are selected based on satisfactory results of multiple removal obtained through this process. In addition, we normalize the data to the amplitude range of -1 to 1 and suppress random noise on the training data before the 3D U-net training.

3. Numerical experiments

In this part the proposed 3D U-net approach is contrasted with the 2D U-net approach and its effectiveness is verified through the utilization of both synthesis and reality data. In the experiments, we use the Keras framework of deep learning to implement the proposed 3D U-net approach on NVIDIA GeForce RTX 2080 Ti GPU.

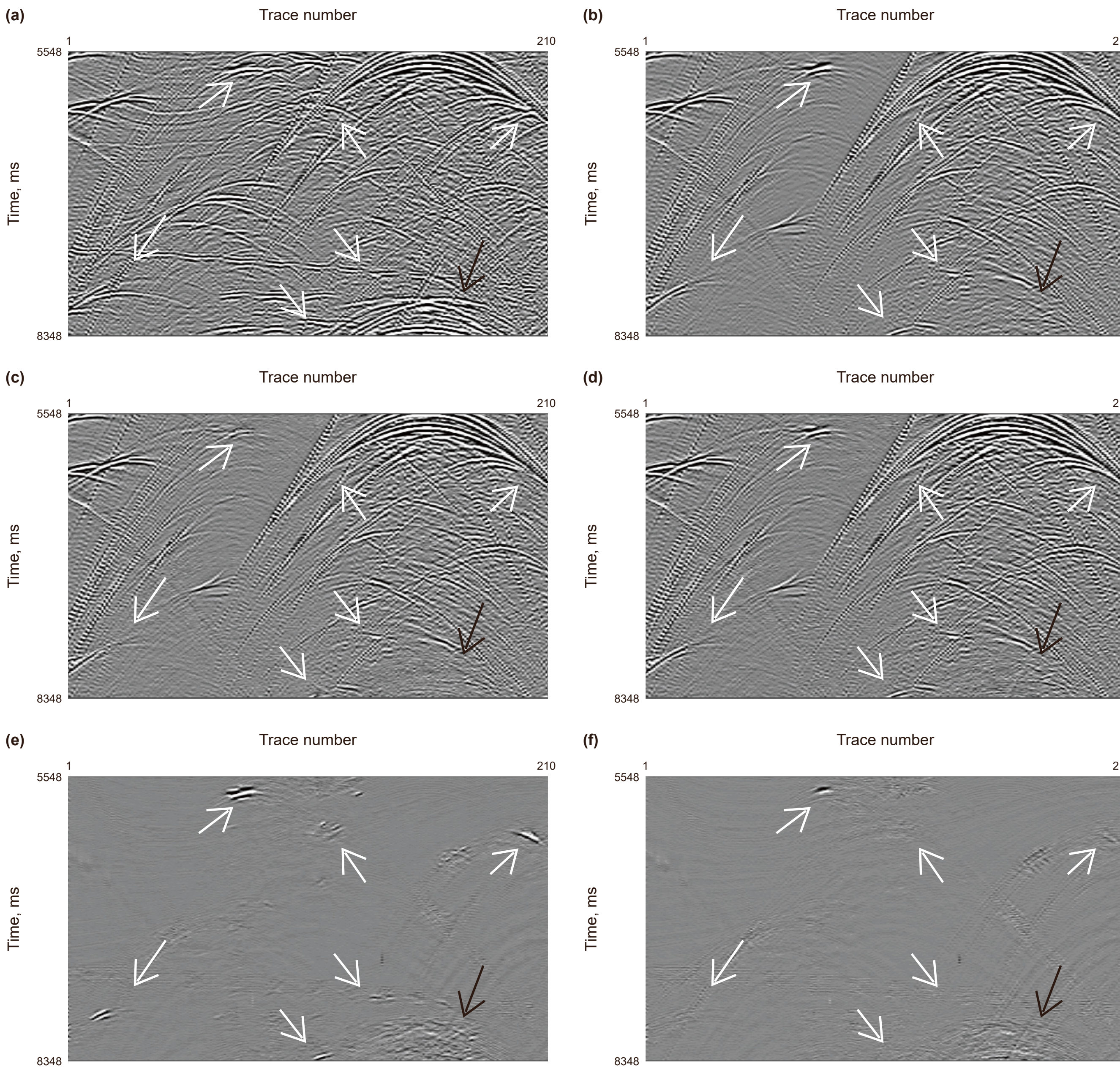

Fig. 8. Amplified results of synthesis data example. **(a)** Initial recorded data. **(b)** Actual primaries. **(c)** Estimable primaries of the 2D U-net approach. **(d)** Estimable primaries of the 3D U-net approach. **(e)** Difference gathers of the 2D U-net approach. **(f)** Difference gathers of the 3D U-net approach.

3.1. The synthesis data

The synthesis data utilized in this section, referred to as Sigsbee2B data, is derived by the SMAART joint venture consortium (Bishop et al., 2001). The synthesis data set consists of 496 common-shot gathers. The receiver interval is 22.86 m and the shot interval is 45.72 m. Each trace in this data set comprises 881 time samples, and the time sampling interval is 8 ms. Fig. 5(a)–(c) depict the initial recorded data, simulated multiples generated by 2D SRME (Verschuur and Berkhout, 1997) and actual primaries in five adjacent common-offset gathers. The displayed parts in Fig. 5(a)–(c) only include 300 traces in each gather from 4948 to 10156 ms.

For the network parameters utilized in both the 2D U-net approach and 3D U-net approach, we choose the size of the convolution kernel as 3×3 and $3 \times 3 \times 3$, respectively. The number of down-sampling step is set to 4, and the count of convolution kernels in the first down-sampling step is chosen as 64 in both two approachs. Moreover, we choose the learning rate of 3×10^{-4}, the epoch number of 20 and the batch size of 6 in both two approaches. The size of 2D data window is set to 16×16 and the size of 3D data window is set to $16 \times 16 \times 5$. This implies that each 3D window is consisted of five 2D windows located at five adjacent gathers. We train the U-net for multiple suppression one gather by one gather in the 2D U-net approach. In the training and prediction process of the synthesis data, the total count of 2D data windows in each gather and the total number of 3D data windows is 11826. Fig. 6(a)–(c) show the estimable primaries, removed multiples and difference gather gotten by subtracting Fig. 6(a) from Fig. 5(c) of the 2D U-net approach in corresponding five gathers. Fig. 7(a)–(c)

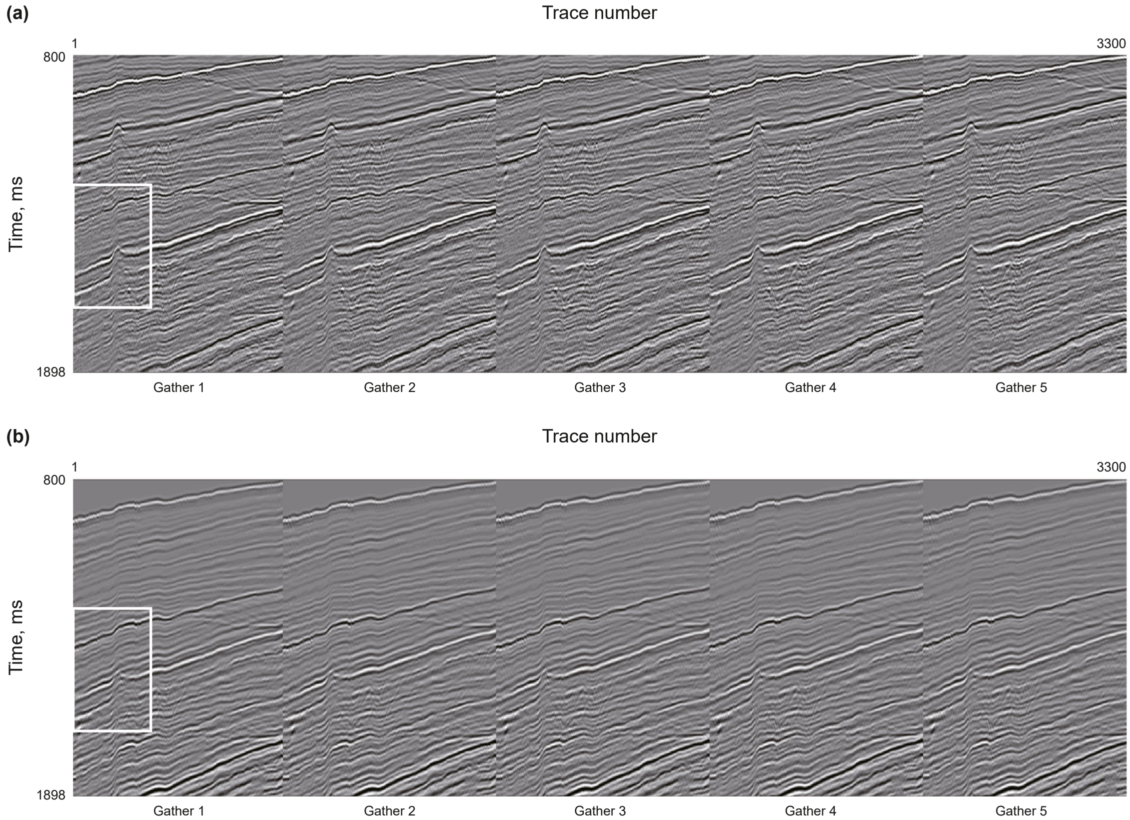

Fig. 9. Reality data example in five gathers. **(a)** The initial recorded data. **(b)** Simulated multiples by 2D SRME.

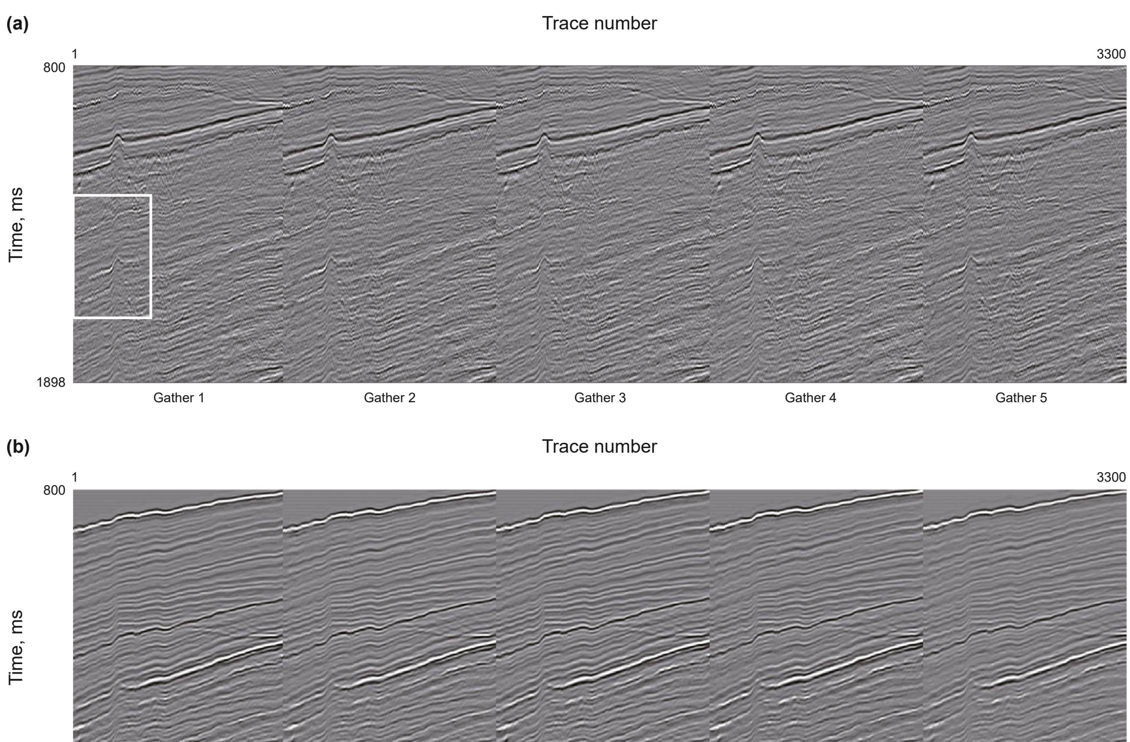

Fig. 10. Reality data example in five gathers. **(a)** Estimable primaries of the 2D U-net approach. **(b)** Removed multiples of the 2D U-net approach.

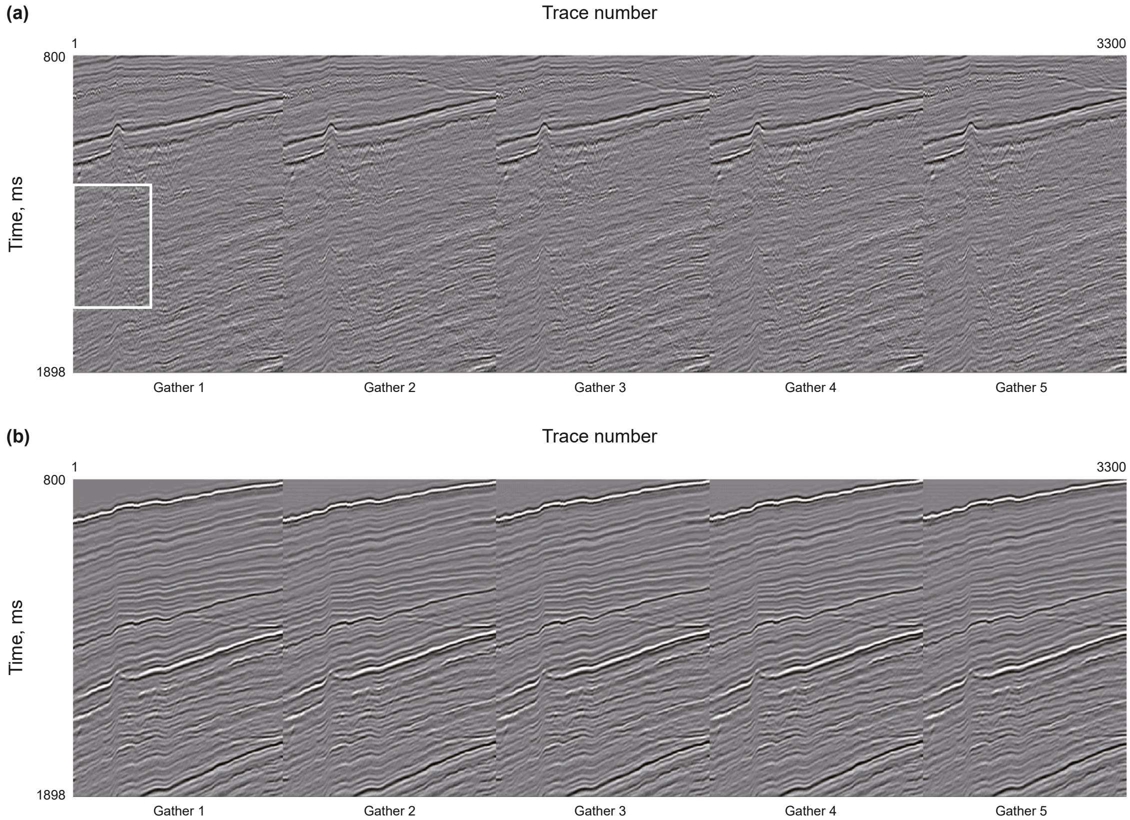

Fig. 11. Reality data example in five gathers. **(a)** Estimable primaries of the 3D U-net approach. **(b)** Removed multiples of the 3D U-net approach.

show the estimable primaries, removed multiples and difference gather gotten by subtracting Fig. 7(a) from Fig. 5(c) of the 3D U-net approach in the same five gathers.

To enhance visibility, we select partial area of one gather for enlarged display. The ranges denoted by the white rectangles in Figs. 5(a), 5(c), 6(a), 6(c), 7(a), and 7(c) are enlarged in Fig. 8(a)–(f). The proposed 3D U-net approach enhances the capability to handle intricate disparities between actual and simulated multiples, as well as preserves the continuity of primaries, owing to its utilization of 3D windows and 3D network modules. The white arrows in Fig. 8(e) and (f) illustrate the superior capability of the 3D U-net approach in preserving primaries contrasted with the 2D U-net approach. Additionally, the black arrows in Fig. 8(e) and (f) attest that the 3D U-net approach exhibits improved effectiveness in eliminating residual multiples compared to the 2D U-net approach.

The signal-to-noise ratio (SNR) is calculated by $SNR = 10\log_{10}\left(\|p_0\|_2^2/\|p-p_0\|_2^2\right)$ to facilitate quantitative comparison of different results, with p_0 and p representing the actual and estimable primaries, respectively. We simultaneously input five gathers of the actual and estimable primaries into the SNR calculation equation to get SNRs of the 2D U-net approach and 3D U-net approach, which are 14.9 and 15.9, respectively. The calculation time of the 2D U-net approach and 3D U-net approach is 4027 and 3230 s, respectively. In the 2D U-net approach, the corresponding calculation time taken for each of the five gathers is 797, 802, 811, 809, and 808 s, respectively. The 2D U-net approach requires sequential training and prediction in each gather, resulting in longer time compared to the 3D U-net approach. Therefore, contrasted with the 2D U-net approach, the 3D U-net approach achieves higher SNR at the cost of less time.

3.2. The reality data

The reality data comprises 2241 common shot gathers, with each gather comprising 240 traces. And each trace comprises 3000 time samples. The time interval is 2 ms. In this part we utilize the common offset gather (offset = 395 m) ranging from 800 ms to 1898 ms with a total of 660 traces per gather to demonstrate the performance of various approaches. Fig. 9(a) and (b) depict the initial recorded data and corresponding simulated multiples by 2D SRME in five adjacent gathers.

The count of convolution kernels is set to 16 in both 2D U-net approach and 3D U-net approach during the initial down-sampling step of U-net. The other network hyper-parameters remain unchanged from those utilized in the synthesis data example. The learning rate is configured as 1×10^{-4}, the batch size is configured as 16 and the epoch number is configured as 40 for these two approaches. The window size is chosen as $16 \times 16 \times 5$ in the 3D U-net approach and 16×16 in the 2D U-net approach. We train the 2D U-net for multiple suppression one gather by one gather. In the training and prediction process of the reality data, the total count of 2D windows in each gather and the total number of 3D windows generated with five gathers is 7998. Fig. 10(a) and (b) depict the estimable primaries and removed multiples of the 2D U-net approach in corresponding five gathers, respectively. Fig. 11(a) and (b) show the estimable primaries and removed multiples of the 3D U-net approach in the same five gathers.

We choose to enlarge partial area of one gather for better comparison. The parts delineated by the white rectangles in Figs. 9(a), 9(b), 10(a) and 11(a) are magnified in Fig. 12. Contrasted with the 2D U-net approach with 2D windows, the 3D U-net approach with 3D windows exhibit superior capability in handling intricate disparities between the actual and simulated multiples.

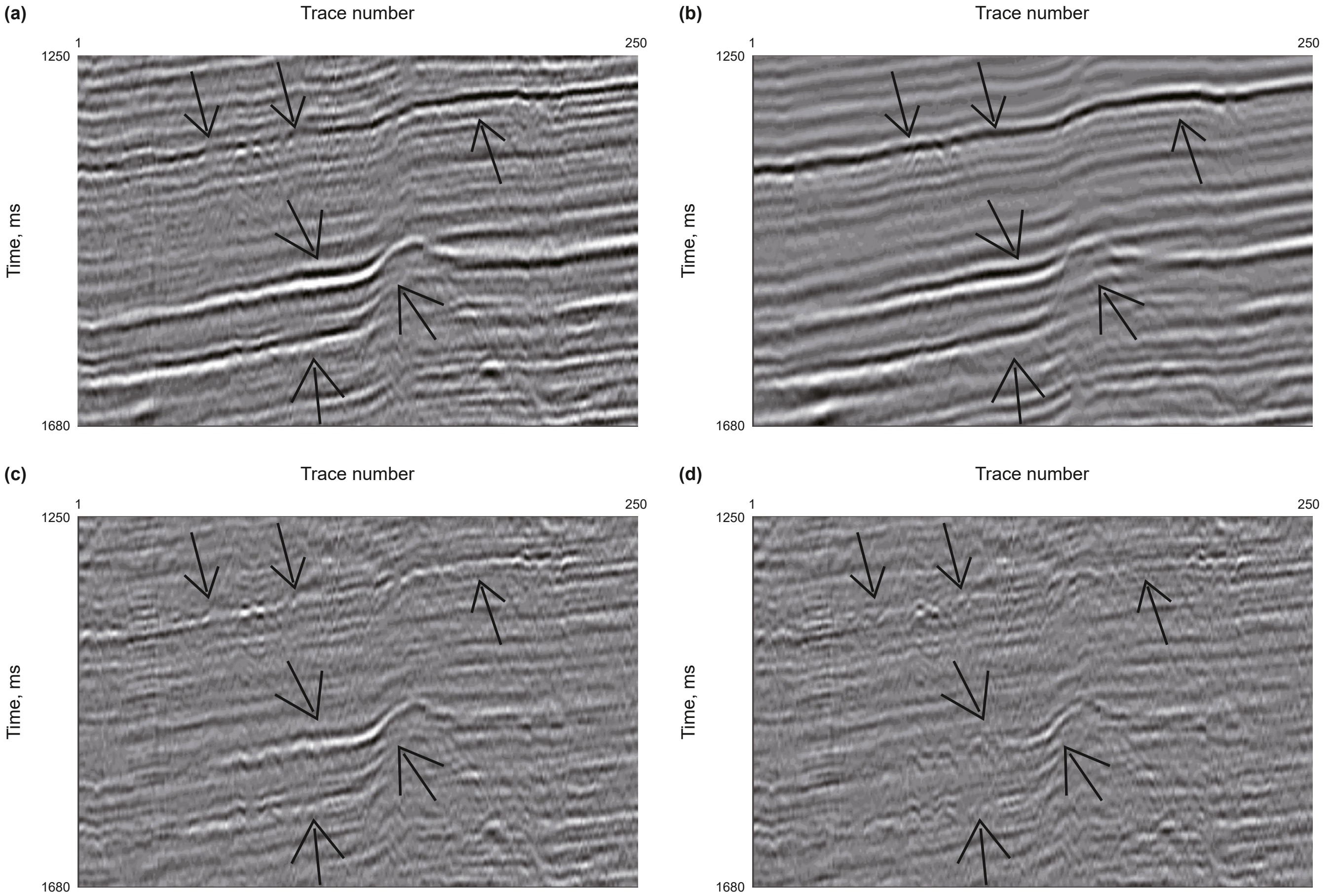

Fig. 12. Amplified results of reality data example. **(a)** Initial recorded data. **(b)** Simulated multiples. **(c)** Estimable primaries of the 2D U-net approach. **(d)** Estimable primaries of the 3D U-net approach.

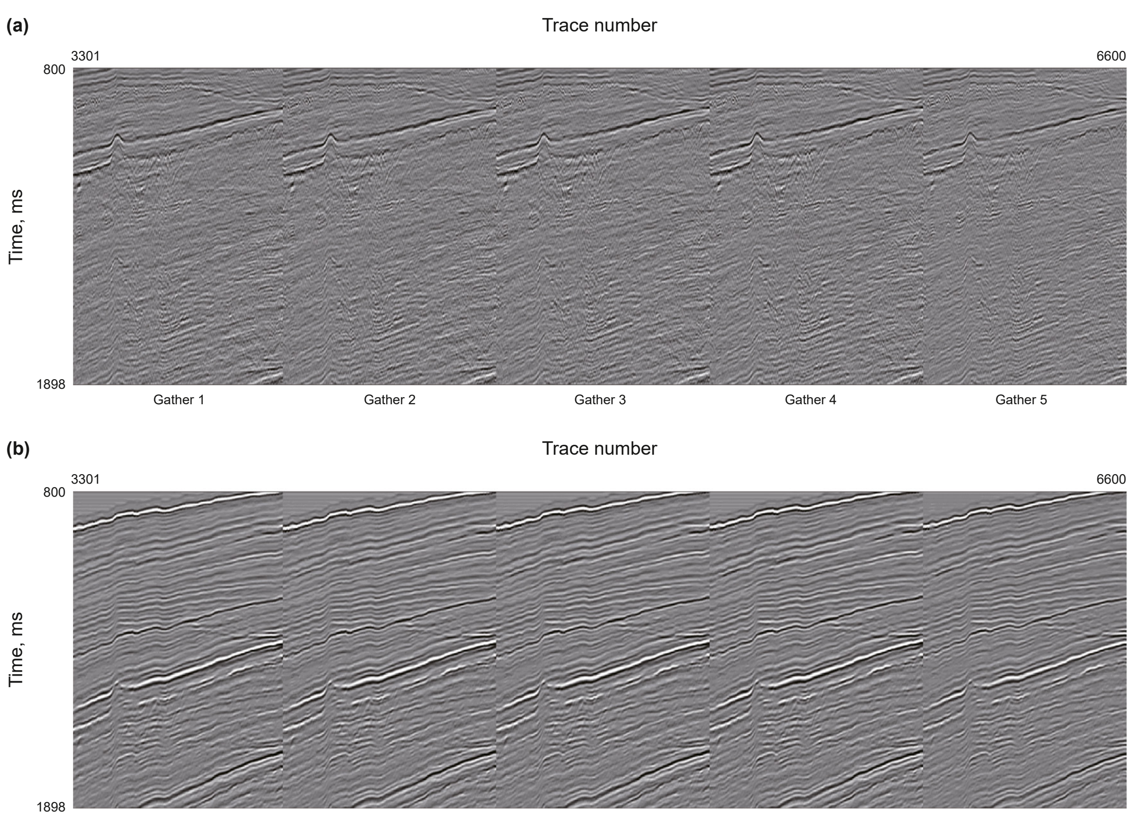

Fig. 13. Reality data example in the fourth data segment with TL. **(a)** Estimable primaries of the 3D U-net approach. **(b)** Removed multiples of the 3D U-net approach.

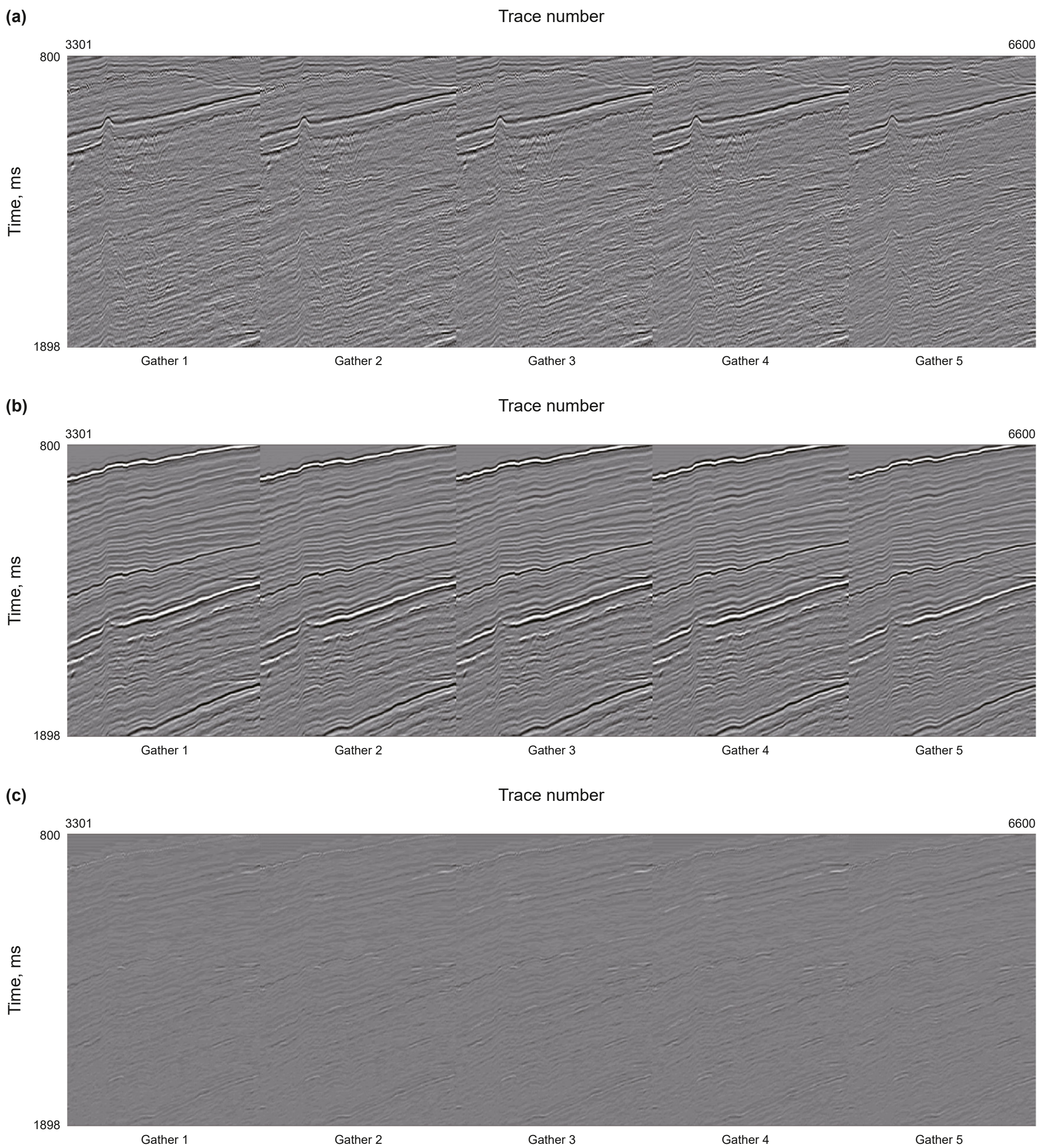

Fig. 14. Reality data example in the fourth data segment without TL. **(a)** Estimable primaries of the 3D U-net approach. **(b)** Removed multiples of the 3D U-net approach. **(c)** Difference gathers gotten by subtracting Fig. 13(a) from Fig. 14(a).

The black arrows in Fig. 12(c) and (d) denote that the proposed 3D U-net approach can eliminate residual multiples more effectively than the 2D U-net approach. The total calculation time required for the 2D U-net approach and the 3D U-net approach is 1335 s and 554 s, respectively. The 3D U-net approach needs less computational time than the 2D U-net approach.

3.3. The transfer learning strategy

We incorporate the TL strategy to further enhance the efficiency of the proposed 3D U-net approach. In the initial data segment comprising five seismic gathers, we partition the data into 3D windows of size $16 \times 16 \times 5$ for 3D U-net training with 40 epochs. The estimable primaries and removed multiples of the first data segment are shown in Fig. 11. Subsequently, we utilize the estimated network parameters of 3D U-net in the previous data segment as the initial network parameters for training 3D U-net with the epoch number of 12 in the next data segment. Each data segment comprises five gathers of the initial recorded data and simulated multiples. Fig. 13(a) and (b) illustrate the estimable primaries and removed multiples in the fourth data segment by the 3D U-net approach with TL. Conversely, if we initialize the network parameters for training the 3D U-net in the fourth data segment with random values drawn from the Gaussian distribution, the resulting estimable primaries and removed multiples are depicted in Fig. 14(a) and (b) by the 3D U-net approach without TL. Fig. 14(c) depicts the seismic gathers obtained by subtracting the estimable primaries in Fig. 13(a) from those in Fig. 14(a). Similar results are observed in the fourth data segment using both the proposed 3D U-net method with TL and the one without TL. Both these two approaches remove multiples effectively. Fig. 15 illustrates the training loss curve versus the epoch number in the fourth data

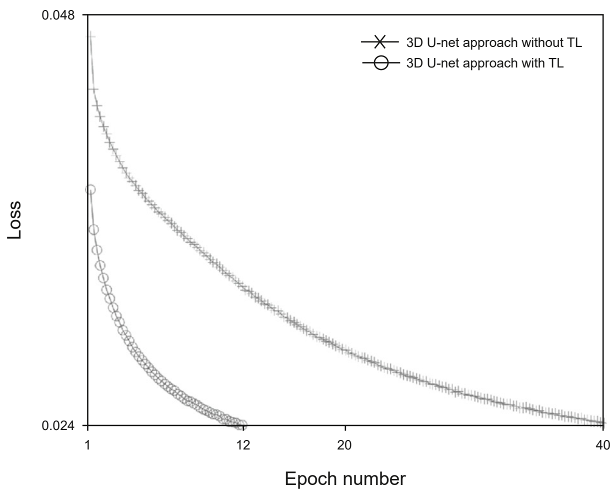

Fig. 15. The training loss curve versus the epoch number.

segment. It is evident that both approaches achieve comparable loss values. The computational time of the 3D U-net approach with TL and the one without TL in the fourth data segment is 166 s and 555 s. The 3D U-net approach with TL can reduce the computational time by 70% contrasted with the one without TL. From the second data segment to the last one the proposed 3D U-net approach with TL requires less computational time compared to the one without TL.

4. Discussion

4.1. Network versatility for multiple removal

In this paper, we improve the multiple suppression accuracy and enhance primary protection effectiveness by adding the dimension of gather to construct 3D U-net and using 3D data windows of training data. In addition, the TL theory has been used to solve the problem of efficiency improvement of multiples suppression in the 2D U-net approach (Li et al., 2023c). For 3D U-net approach the TL strategy can also be introduced to improve its efficiency.

Wang et al. (2022a) proposed the self-supervised deep neural network (DNN) combined with the adaptive virtual events (AVEs) approach. The AVE approach is used to get the simulated multiples and the self-supervised learning with the DNN is conducted to estimate primaries. The iterative steps of the fast iterative shrinkage thresholding algorithm (FISTA) are unfolded in order to construct FISTA-Net, which takes the initial recorded data and simulated multiples as input data and outputs estimable primaries (Li et al., 2023b). Moreover, FISTA-Net incorporates the non-linear mapping capability of U-net into its architecture. Both these approaches and the proposed 3D U-net approach use self-supervised learning and do not require labels of primaries produced by the SRME approach (Verschuur and Berkhout, 1997). In the future work we will conduct comparative studies based on diversified network architectures such as FISTA-Net (Li et al., 2023b), DNN (Wang et al., 2022a) and network of ensemble learning (Wang et al., 2022b) with 3D data windows as the training data. Whether we can achieve better suppression effect of seismic surface-related multiples

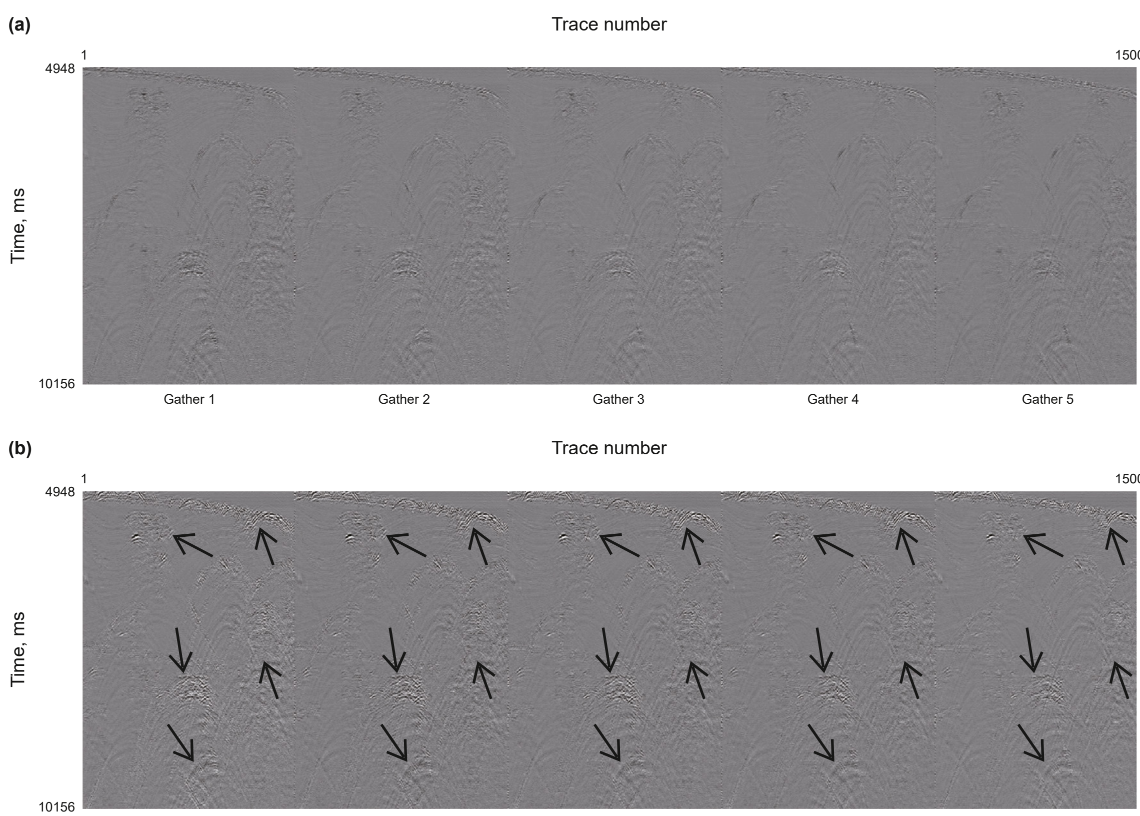

Fig. 16. Synthesis data example in five gathers. **(a)** Difference gathers with little temporal shift (five-time samples). **(b)** Difference gathers with significant temporal shift (ten-time samples).

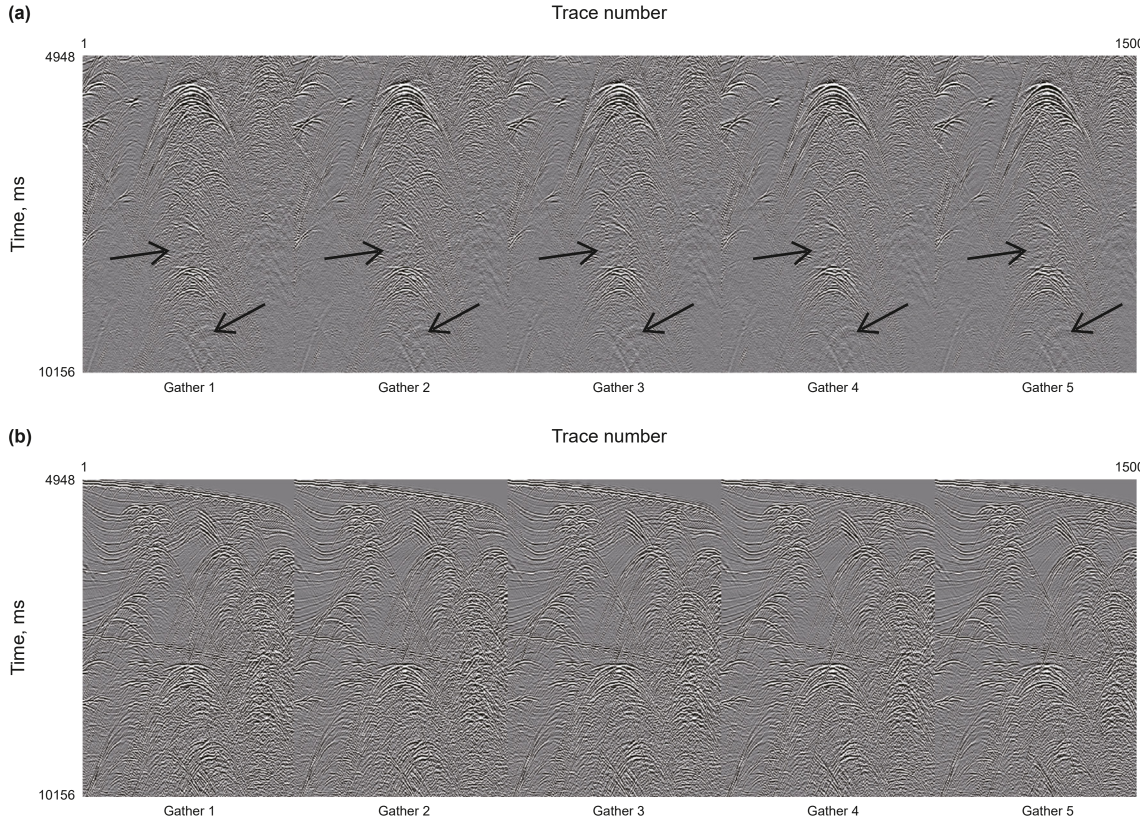

Fig. 17. Synthesis data example in five gathers. **(a)** Estimable primaries of the traditional LR approach. **(b)** Removed multiples of the traditional LR approach.

remains to be verified, and we will evaluate the performance of different networks in the future work.

4.2. Selection of number of gathers

In the proposed 3D U-net approach, several gathers need to be divided into 3D windows to train 3D U-net in each data segment. We select an important parameter of the number of gathers by the way of trial and error. With smaller number of gathers the 3D windows can not represent the spatial continuity and anisotropy of seismic events in the gather direction effectively. With larger number of gathers the mismatches between the simulated and true multiples may be too complex in 3D windows. And in this case the 3D U-net can not remove these mismatches effectively. For the synthetic data the SNRs of estimable primaries are 15.1, 15.6, 15.9 and 15.3 when the number of gathers is selected as 1, 3, 5 and 8 in each data segment, respectively. The SNR is obtained by inputting the corresponding number of gathers of the actual and estimable primaries into the SNR calculation equation simultaneously. The comparison results show that the SNR of estimable primaries is highest when the number of gathers is selected as 5. The corresponding estimable primaries, removed multiples and difference gather are shown in Fig. 7.

4.3. Handling complex multiple differences

The temporal shift exists between the simulated multiples in Fig. 5(b) and the actual multiples in the initial recorded data in Fig. 5(a). We systematically increase the temporal shift of the simulated multiples to assess its impact on multiple suppression accuracy. After increasing five-time samples of travel time from the simulated multiples in Fig. 5(b), we adaptively subtract them from the initial data to obtain the corresponding estimable primaries, which are subtracted from Fig. 5(c) to give the difference gathers in Fig. 16(a). The difference gathers in Fig. 16(a) are similar to those shown in Fig. 7(c). By introducing little temporal shifts (five-time samples) to the simulated multiples, the proposed 3D U-Net approach still achieves fine results of multiple removals. In Fig. 5(b), we increase the travel time of the simulated multiples using ten-time samples and obtain the corresponding estimable primaries, which are subtracted from Fig. 5(c) to give the difference gathers in Fig. 16(b). The events indicated by the black arrows in Fig. 16(b) are caused by residual multiples. The SNRs of the estimable primaries corresponding to Fig. 16(a) and (b) are 15.4 and 14.7, respectively. The proposed 3D U-Net approach is unable to effectively handle significant temporal shifts (ten-time samples), resulting in noticeable residual multiples.

4.4. Contrast with traditional LR approach

The 3D U-net approach proposed in this paper is aimed at the adaptive subtraction process of SRME (Verschuur and Berkhout, 1997). The LR approach (Guitton and Verschuur, 2004; Li and Li, 2018) is usually used to conduct adaptive subtraction. We use the synthesis data for comparative experiments. Fig. 17(a) is the estimable primaries of the traditional LR approach and Fig. 17(b) is the removed multiples. The black arrows in Figs. 7(a) and 17(a) show that there are obvious residual multiples caused by the traditional LR approach. We simultaneously input five gathers of the actual and estimable primaries into the SNR calculation equation to get the SNR of the traditional LR approach, which is 12.8. The calculation time of traditional LR approach is only 116 s. The SNR and calculation time of the proposed 3D U-net approach is 15.9 and 3230 s. Compared with the traditional LR approach, the proposed

3D U-net approach has lower computational efficiency, but improves the precision of multiple suppression.

4.5. Summary of innovation points

In order to further improve the precision of multiple suppression, we propose an adaptive subtraction approach using 3D U-net architecture, which can adaptively separate primaries and multiples utilizing 3D windows. The contribution of this paper can be summarized as two points:

(1) The utilization of 3D windows allows for enhanced depiction of spatial continuity and anisotropy of seismic events along the gather direction in comparison to 2D windows.
(2) The 3D U-net approach with 3D network modules can effectively preserve the continuity of primaries and improve effectiveness in managing the complex disparities between the actual and simulated multiples in 3D windows. In addition, we introduce the TL strategy in the proposed 3D U-net approach in order to expedite the network training.

5. Conclusion

In this paper we present an adaptive subtraction approach utilizing 3D U-net, with the aim of improving the accuracy of seismic multiple suppression and enhancing primary protection effectiveness. In comparison to the 2D U-net approach, the proposed 3D U-net approach utilizes 3D network modules with 3D data windows as the training data. The 3D U-net approach can enhance the ability to handle the complex disparities between the actual and simulated multiples while preserving the continuity of primaries. And the 3D U-net approach proposed in this paper demonstrates superior performance in safeguarding primaries and eliminating residual multiples contrasted with the 2D U-net approach. Moreover, we incorporate the TL theory, leveraging the estimated network parameters of 3D U-net in the previous data segment as the initial network parameters for training 3D U-net in the subsequent data segment. Consequently, the proposed 3D U-net approach can be expedited with reduced epoch number of network training. We will explore semi-supervised training by incorporating some gathers of actual primaries in the future work. This could potentially further improve the performance of the 3D U-net approach, especially in reality data application, in which the estimable primaries by the traditional approach can be used as the pseudo-labels (Lee, 2013).

CRediT authorship contribution statement

Jin-Qiang Huang: Writing – review & editing, Writing – original draft, Software, Methodology. **Li-Yun Fu:** Writing – review & editing, Validation, Software. **Jia-Hui Ma:** Writing – original draft, Validation, Methodology. **Xing-Zhong Du:** Writing – review & editing, Methodology. **Zhong-Xiao Li:** Writing – review & editing, Writing – original draft, Supervision, Methodology, Formal analysis. **Ke-Yi Sun:** Writing – review & editing, Methodology.

Declaration of competing interest

The authors declare that they have no known competing financial interests or personal relationships that could have appeared to influence the work reported in this paper.

Acknowledgments

This work was supported by National Natural Science Foundation of China (42364008, 41804110), in part by Guizhou Provincial Basic Research Program (Natural Science) (ZK[2022]060), in part by China Postdoctoral Science Foundation (2022M723127) and in part by Youth Innovation Team Project of Shandong Provincial Education Department (2022KJ141).

References

Bishop, K., et al., 2001. Investigation of vendor demultiple technology for complex subsalt geology. In: 71th Annual International Meeting, SEG, Expanded Abstracts. https://doi.org/10.1190/1.1816327.

Guitton, A., Verschuur, D.J., 2004. Adaptive subtraction of multiples using the L1-norm. Geophys. Prospect. 52 (1), 27–38. https://doi.org/10.1046/j.1365-2478.2004.00401.x.

Kingma, D.P., Ba, J.L., 2015. Adam: a method for stochastic optimization. In: 3rd International Conference for Learning Representations. https://doi.org/10.48550/arXiv.1412.6980.

Lee, D., 2013. Pseudo-Label: the simple and efficient semi-supervised learning method for deep neural networks. Proceedings of the 30th International Conference on Machine Learning. https://api.semanticscholar.org/CorpusID:18507866.

Li, Z., Sun, N., Gao, H., Qin, N., Li, Z., 2021. Adaptive subtraction based on U-net for removing seismic multiples. IEEE Trans. Geosci. Rem. Sens. 59 (11), 9796–9812. https://doi.org/10.1109/TGRS.2021.3051303.

Li, Z., Sun, N., Zeng, T., Zhang, H., Tian, J., 2023a. Adaptive subtraction based on the matching filter with three frequency bands of modeled multiples for removing seismic multiples. Geosci. Rem. Sens. Lett. IEEE 20. https://doi.org/10.1109/LGRS.2023.3261059.

Li, Z., Sun, K., Zeng, T., Ma, J., Qi, Z., Sun, N., Wang, Y., 2023b. Unsupervised FISTA-Net-based adaptive subtraction for seismic multiple removal. IEEE Trans. Geosci. Rem. Sens. 61. https://doi.org/10.1109/TGRS.2023.3306511.

Li, Z., Ma, J., Qi, Z., Zhang, L., Xie, F., Yang, J., 2023c. Accelerating the U-net based adaptive subtraction with transfer learning for removing seismic multiples in field data. J. Seismic Explor. 32, 373–384.

Li, Z., Li, Z., 2018. Accelerated 3D blind separation of convolved mixtures based on the fast iterative shrinkage thresholding algorithm for adaptive multiple subtraction. Geophysics 83 (2), V99–V113. https://doi.org/10.1190/geo2016-0384.1.

Liu, J., Hu, T., Peng, G., 2018. Suppressing seismic inter-bed multiples with the adaptive virtual events method. Chin. J. Geophys. 61 (3), 1196–1210. https://doi.org/10.6038/cjg2018L0663 (in Chinese).

Ma, J., Sen, M.K., Chen, X., 2009. Free-surface multiple attenuation using inverse data processing in the coupled plane-wave domain. Geophysics 74 (4), V75–V81. https://doi.org/10.1190/1.3137059.

Ma, J., Zhao, K., Liao, Z., 2024a. A fast amplitude preserving three-parameter 3D parabolic Radon transform and its application on multiple attenuation. Petrol. Sci. https://doi.org/10.1016/j.petsci.2024.06.011.

Ma, J., Sun, K., Dai, X., Li, B., Wang, Y., Li, Z., 2024b. U-Net based adaptive subtraction utilizing three frequency-bands of simulated multiples for their suppression. Geosci. Rem. Sens. Lett. IEEE. https://doi.org/10.1109/LGRS.2024.3381078.

Mehta, R., Arbel, T., 2018. 3D U-Net for brain tumour segmentation. International MICCAI Brainlesion Workshop 11384, 254–266. https://doi.org/10.1007/978-3-030-11726-9_23.

Mousavi, S.M., Beroza, G.C., 2022. Deep-learning seismology. Science 377 (6607), eabm4470. https://doi.org/10.1126/science.ahm4470.

Ronneberger, P., Fischer, P., Brox, T., 2015. U-Net: convolutional networks for biomedical image segmentation. In: International Conference on Medical Image Computing and Computer-Assisted Intervention-MICCAI 2015. https://doi.org/10.1007/978-3-319-24574-4_28.

Siahkoohi, A., Louboutin, M., Herrmann, F.J., 2019. The importance of transfer learning in seismic modeling and imaging. Geophysics 84 (6), A47–A52. https://doi.org/10.1190/geo2019-0056.1.

Sheng, G., Yang, S., Tang, X., Guo, X., 2022. Arrival-time picking of microseismic events based on MSNet. Geophysics 87 (2), KS57–KS71. https://doi.org/10.1190/geo2020-0469.1.

Song, H., Mao, W., Tang, H., 2021. Application of deep neural networks for multiples attenuation. Chin. J. Geophys. 64 (8), 2795–2808. https://doi.org/10.6038/cjg2021O0369 (in Chinese).

Senapati, P., Basu, A., Deb, M., Dhal, K.G., 2023. Sharp dense U-Net: an enhanced dense U-Net architecture for nucleus segmentation. Appl. Geophys. 15, 2079–2094. https://doi.org/10.1007/s13042-023-02017-y.

Verschuur, E., 2013. Seismic Multiple Removal Techniques: Past, Present and Future. EAGE Publications, Houten, Netherlands. https://doi.org/10.3997/9789073834965.

Verschuur, D.J., Berkhout, A.J., 1997. Estimation of multiple scattering by iterative inversion, part II: practical aspects and examples. Geophysics 62 (5), 1596–1611. https://doi.org/10.1190/1.1444262.

Wang, K., Hu, T., Wang, S., 2022a. Unsupervised learning for seismic internal multiple suppression based on adaptive virtual events. IEEE Trans. Geosci. Rem. Sens. 60. https://doi.org/10.1109/TGRS.2022.3169481.

Wang, K., Hu, T., Zhao, B., 2022b. An unsupervised deep neural network approach based on ensemble learning to suppress seismic surface-related multiples. IEEE Trans. Geosci. Rem. Sens. 60. https://doi.org/10.1109/TGRS.2022.3225809.

Wang, K., Hu, T., Zhao, B., Wang, S., 2023a. An unsupervised learning method to suppress seismic internal multiples based on adaptive virtual events and joint

constraints of multiple deep neural networks. IEEE Trans. Geosci. Rem. Sens. 61. https://doi.org/10.1109/TGRS.2023.3243106.
Wang, K., Hu, T., Zhao, B., Wang, S., 2023b. Surface-related multiple attenuation based on a self-supervised deep neural network with local wavefield characteristics. Geophysics 88 (5), V387–V402. https://doi.org/10.1190/geo2022-0599.1.
Wu, X., Liang, L., Shi, Y., Fomel, S., 2019. FaultSeg3D: using synthetic data sets to train an end-to-end convolutional neural network for 3D seismic fault segmentation. Geophysics 84 (3), IM35–IM45. https://doi.org/10.1190/geo2018-0646.1.
Wang, K., Hu, T., Liu, X., Wang, S., Wei, J., 2021. Suppressing seismic multiples based on the deep neural network method with data augmentation training. Chin. J. Geophys. 64 (11), 4196–4214. https://doi.org/10.6038/cjg2021O0517 (in Chinese).
Wang, Y., Lu, W., Liu, J., Zhang, M., Miao, Y., 2019. Random seismic noise attenuation based on data augmentation and CNN. Chin. J. Geophys. 62 (1), 421–433. https://doi.org/10.6038/cjg2019M0385 (in Chinese).
Xue, L., Xu, S., Nie, J., Qin, J., Han, J., Liu, Y., Liao, Q., 2024. An efficient data-driven global sensitivity analysis method of shale gas production through convolutional neural network. Petrol. Sci. https://doi.org/10.1016/j.petsci.2024.02.010.
Yang, N., Li, G., Li, T., Zhao, D., Gu, W., 2023. An improved deep dilated convolutional neural network for seismic facies interpretation. Petrol. Sci. https://doi.org/10.1016/j.petsci.2023.11.027.
Zhang, J., Sheng, G., 2020. First arrival picking of microseismic signals based on nested U-Net and Wasserstein Generative Adversarial Network. J. Petrol. Sci. Eng. 195, 107527. https://doi.org/10.1016/j.petrol.2020.107527.
Zhao, M., Chen, S., Dave, Y., 2019. Waveform classification and seismic recognition by convolution neural network. Chin. J. Geophys. 62 (1), 374–382. https://doi.org/10.6038/cjg2019M0151 (in Chinese).